Zweitveröffentlichung/
Secondary Publication

Staats- und Universitätsbibliothek Bremen

https://media.suub.uni-bremen.de

Siham OUMMADI, Benoit Nait-Ali, Arnaud Alzina, Jean-Louis Victor, Yann Launay, Mojtaba Mirdrikvand, Wolfgang Dreher, Kurosch Rezwan, David S. Smith

Distribution of water in ceramic green bodies during drying

Journal Article as: peer-reviewed accepted version (Postprint)

DOI of this document*(secondary publication): https://doi.org/10.26092/elib/2509

Publication date of this document: 20/10/2023

* for better findability or for reliable citation

Recommended Citation (primary publication/Version of Record) incl. DOI:

Siham OUMMADI, Benoit Nait-Ali, Arnaud Alzina, Jean-Louis Victor, Yann Launay, Mojtaba Mirdrikvand, Wolfgang Dreher, Kurosch Rezwan, David S. Smith,
Distribution of water in ceramic green bodies during drying,
Journal of the European Ceramic Society, Volume 39, Issue 10, 2019, Pages 3164-3172, ISSN 0955-2219,
https://doi.org/10.1016/j.jeurceramsoc.2019.04.005

Please note that the version of this document may differ from the final published version (Version of Record/primary publication) in terms of copy-editing, pagination, publication date and DOI. Please cite the version that you actually used. Before citing, you are also advised to check the publisher's website for any subsequent corrections or retractions (see also https://retractionwatch.com/).

This document is made available under a Creative Commons licence.

The license information is available online: https://creativecommons.org/licenses/by-nc-nd/4.0/

Take down policy

If you believe that this document or any material on this site infringes copyright, please contact publizieren@suub.uni-bremen.de with full details and we will remove access to the material.

Distribution of water in ceramic green bodies during drying

Siham OUMMADI[a], Benoit Nait-Ali[a], Arnaud Alzina[a], Jean-Louis Victor[a], Yann Launay[a], Mojtaba Mirdrikvand[b], Wolfgang Dreher[b], Kurosch Rezwan[c], David S. Smith[a]

[a] University of Limoges, IRCER, UMR CNRS 7315, 12 rue Atlantis, F-87068 Limoges, France
[b] University of Bremen, Department of Chemistry (FB2), in vivo MR Group, Leobener Str. 7, 28359 Bremen, Germany
[c] University of Bremen, Advanced Ceramics, Am Biologischen Garten 2, IW3, 28359 Bremen, Germany

ARTICLE INFO

Keywords:
Distribution of water
Drying
Multi-scale
Alumina
Kaolin

ABSTRACT

In order to investigate drying mechanisms at different stages, the distribution of water within the ceramic green bodies at different scales has been examined. The experimental measurements, using a simple weighing technique and Magnetic Resonance Imaging (MRI), show that during the first stage of drying involving shrinkage the material is constituted of uniquely solid and water with no gradient in water content within the sample. Then, during the second stage of drying, significant differences of water content as a function of position appear. As a complement, at the grain scale, observations using environmental scanning electron microscopy were made giving useful information on the solid–liquid–gas interfaces in the near surface part of the green body. Finally, the gradients in the water distribution were exploited to make a simple estimate of the diffusion coefficient of water with its dependence on the moisture content.

1. Introduction

Water is often incorporated into a ceramic material to aid forming into a complex shape [1,2]. But then this water must be removed before the firing step to avoid damage due to trapped water vapour expanding [2]. Convective drying of ceramic products is therefore an important process step in their manufacture. There are two main problems related directly to drying which can motivate studies. First, it requires a significant consumption of energy. In this respect, according to the French law number 2015-992 and various European directives, industry will be complied to reduce energy consumption by 50% before the end of 2050 [3]. The second important point is that mechanical stresses occur within the material during drying due to water removal and shrinkage. This may create warping or cracks in the final product if the drying conditions are not carefully chosen and controlled [4].

Further progress in the understanding of drying mechanisms starts with answering the questions as to exactly how conditions of drying influence the macroscopic water concentration within the solid, and where the liquid is physically located at different scales during drying. Such information is also important for the construction of numerical models of the drying body. A robust and accurate model will be a valuable tool for process optimization.

Drying of ceramic green bodies has already been studied in some detail in the literature [5–9]. To illustrate, convective drying is not only a mechanism to remove water at the surface of the material, but it is also connected to the movement of liquid within the material, either as liquid or in vapour form [5]. Indeed, for drying of granular materials in an environment with constant conditions, i.e. humidity and temperature of the drying-air remain stable, three stages corresponding to different drying rates can be identified [5,6]. In the first one, named the constant-rate period (CRP), the drying rate is independent of the water content and the type of the material. Since the liquid/air interface, where evaporation occurs, remains at the surface of the porous body, the volume decrease of the body simply corresponds to the evaporated liquid. The second step named the first falling-rate period (1stFRP), is very often described by a proportionality between the rate of evaporation and the water content. Body shrinkage has essentially stopped. During this period, evaporation still occurs from the surface but this is no longer behaving as a free water surface. The evaporated liquid is replaced by air. Further removal occurs by evaporation within the porous body where liquid evaporates within the pores and the vapor is transported by diffusion. The final step is the second falling-rate period (2ndFRP), with a non-linear relation between drying rate and moisture content. During this final period, evaporation occurs within the porous body so that the vapour reaches the surface by diffusing through the pores.

In the simplest case, that is without considering the shrinkage of the material, the mechanisms described above have already been investigated in some detail. For example, in the study of drying porous media using Magnetic Resonance Imaging (MRI) [10], the distribution

E-mail address: benoit.nait-ali@unilim.fr (B. Nait-Ali).

https://doi.org/10.1016/j.jeurceramsoc.2019.04.005
Received 14 December 2018; Received in revised form 28 March 2019; Accepted 3 April 2019
Available online 05 April 2019
0955-2219/ © 2019 Elsevier Ltd. All rights reserved.

of air and liquid interacting with colloid particles within an unsaturated solid porous structure as a function of time was observed. The results show that during drying, the particles move to the surface of the sample and congregate in the remaining liquid films adsorbed on the solid. Another study was carried out using MRI on the distribution of a liquid within a porous cylindrical catalyst support pellet. The major aim of this study was to deduce the diffusivity of water as a function of liquid content [11]. Both studies demonstrate that during drying, even in different conditions, gradients in water concentration develop within the porous solid.

The present work focuses on the drying of two technologically important ceramic materials, alumina and kaolin, in a situation which is close to that encountered practically in ceramic processing. The shrinkage behaviour of the ceramic body is therefore an important aspect. Three different techniques, of which two are modern, are used to follow the evolution of water distribution at different scales during the drying process. The first approach is destructive in that weight measurements are made on small blocks cut out of original samples after drying for different periods in time. Results are correlated with those of linear shrinkage. The second complimentary approach uses Magnetic Resonance Imaging (MRI) to give information on the macroscopic distribution of water in the green body with a spatial resolution, better than 0.5 mm. Lastly, given that the major evaporation of water takes place at the surface, observations with the Environmental Scanning Electron Microscope (ESEM) indicate the location of water at the micron scale in the pore/grain microstructure at different instants during drying.

2. Materials and methods

2.1. Sample preparation

Three raw materials were used in this study: two alumina powders with different grain size distributions and a clay powder. The alumina powders were supplied by the Pechiney company. The first one, named P172SB, was chosen for its small grain size, represented by a median size of 0.4 µm, which is suitable for the shaping process of casting. Its surface area, measured using the BET method, is 7.5 $m^2 g^{-1}$. The true density of 3.96 g cm^{-3} was measured with a helium pycnometer and is close to the theoretical density of 3.98 g cm^{-3}. The second alumina, named P152SB, has a larger grain size, with a median size of 1.3 µm and a surface area of 2.6 $m^2 g^{-1}$. This alumina was chosen in order to assess by comparison if any effect of powder granulometry on drying behaviour could be detected. The third raw material which is a clay powder called BIP kaolin, is typically used for traditional ceramic products and supplied by Imerys Ceramic France after extraction from the Beauvoir site. The measured specific surface area of BIP Kaolin is 10 $m^2 g^{-1}$. The median grain size measured using laser light scattering (Mavern Mastersizer 2000) is 9.5 µm. Regarding the value of the specific surface area of kaolin powder, it can be noted that the grains are constituted of agglomerated particles.

Initially, each powder was mixed with water according to the mass quantities in Table 1a. The mixture was stirred in a jar mill (FAURE Equipement) for 75 min with a rotation speed of 35 rpm (Fig. 1, step 1), in order to obtain a homogeneous slurry without any clumps. With the aim of manipulating the mixture and obtaining a homogeneous ceramic paste, the mixture was cast manually on a porous plasterboard and maintained there for approximately 20 min to absorb a part of the initial water (Fig. 1, steps 2 and 3). The paste was cut into samples with the desired dimensions (Fig. 1, step 4). This step proved to be difficult for smaller dimensions; in which case a removable mold was then used to shape samples. Finally, to avoid any premature evaporation before the drying study, the samples were covered with a waterproof plastic film (polyvinyl film used conventionally in kitchens) and placed in an atmosphere saturated in water vapor (Fig. 1, step 5). As the plaster absorbed a part of the slurry water, the obtained samples have a liquid weight percentage which is less than that of the initial composition. The shaped samples final composition before drying is given in Table 1b.

Table 1
(a) Water content in weight percentage in the initial suspensions. (b) Water content in weight percentage in ceramic paste samples.

	Solid (%)	Water (%)
(a) Alumina (P172SB and P152SB)	50	50
Kaolin	35	65
	Solid (%w)	**Water (%w)**
(b) Alumina (P172SB and P152SB)	~70	~30
Kaolin	~60	~40

2.2. Macroscopic scale (~cm): weight loss and linear shrinkage measurements

2.2.1. Weight loss measurements

The evolution of moisture content in alumina and kaolin green bodies was followed at different positions as a function of time with the following procedure. Drying was performed in an oven (SECASI technologies) at a temperature of 40 °C without controlling relative humidity but which was measured at 15%. The sample (15 mm × 15 mm × 40 mm) was placed in the oven. Only one face (15 mm × 15 mm) was exposed to drying and the other faces were covered with polyvinyl film. Then the sample was removed at a precise time t and cut into four sub-samples (Fig. 2). Afterwards, the weights of the different sub-samples were measured before the sub-samples were placed in another oven (PROLABO) for 24 h at 110 °C. Their weight was then measured again after complete drying. The moisture content of each sub-sample at time t was calculated with the relation:

$$X(t) = 100\% \times \frac{w(t) - w_d}{w_d} \quad (1)$$

$X(t)$ is the water content/dry basis, $w(t)$ is the sample weight at time t, and w_d is the sample weight dried at 110 °C for 24 h.

2.2.2. Linear shrinkage measurements

The shrinkage of the samples was evaluated in an instrumented climatic chamber. The sample is placed on a support connected to an instrumented balance with an accuracy of 10^{-3} g. A Linear Variable Differential Transformer sensor (LVDT) supplied by Meggitt Sensorex, which measures the variation of length over time with an accuracy of 5×10^{-6} m, was placed on the sample. The length change is given by:

$$\Delta L = 100\% \times \frac{L(t) - L_d}{L_d} \quad (2)$$

where L_d is the length of the sample at the end of drying, and $L(t)$ is the length of the sample at time t.

2.3. Macroscopic scale (~mm): Zero Echo Time (ZTE) magnetic resonance imaging (MRI)

Magnetic resonance imaging (MRI) measurements were conducted by an optimized Zero Echo Time (ZTE) MRI pulse sequence [12–14] implemented on a 7-Tesla preclinical MRI system (Biospec 70/20, Bruker Biospin GmbH, Ettlingen, Germany). The ZTE method was chosen for the MRI study of water in ceramic samples because of the very short effective transverse relaxation times (T_2*) involved. Background signals originate from NMR hardware components (e.g., supporting material and electronic parts of the RF coil) outside of the Field-of-View (FOV) and thus unwanted wave-pattern image artefacts were removed by applying an Outer Volume Suppression (OVS) module prior to RF excitation of the sample [15]. In ZTE-MRI, for a series of

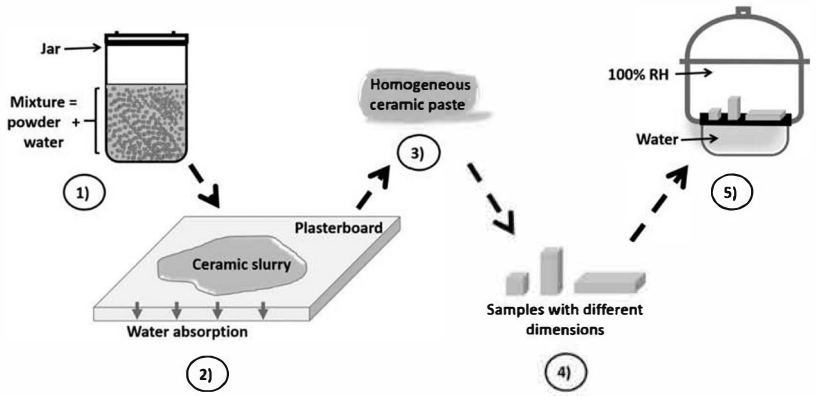

Fig. 1. Representation of the different steps in sample preparation.

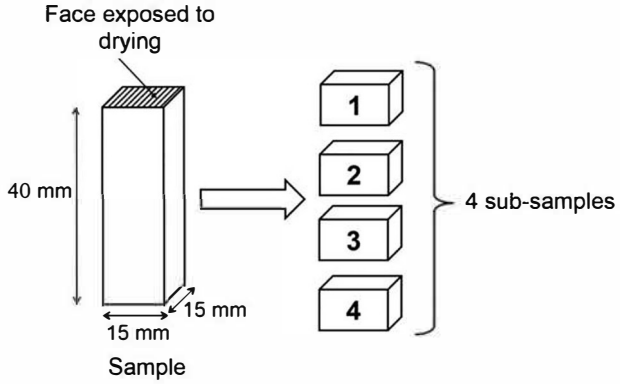

Fig. 2. Representation of the sample divided into 4 blocks.

measurements with short repetition time TR, data are acquired from the whole sample but with different orientations of the applied magnetic field gradient, allowing the reconstruction of a 3D image. In this study, ZTE MRI was performed with a FOV of 48 mm × 48 mm × 48 mm and a matrix size of 128 × 128 × 128, yielding a voxel size of 375 µm × 375 µm × 375 µm. Using a TR of 11.3 ms and 51896 data acquisitions, the total measurement time per 3D image was about 10 min.

Image reconstruction was performed on the MRI console using the software Paravision 5.1 provided by the manufacturer. The 3D MR images were reconstructed by a gridding algorithm to determine the data on a Cartesian grid from the radially sampled k-space data, followed by a 3D Fast Fourier Transformation. It is important to note that some intensity distortions may occur in ZTE images, i.e. a non-uniform intensity distribution may be reconstructed for a uniform object. These image artifacts can be caused by experimental problems (missing or distorted signals near the k-space center acquired immediately after switching from transmission to reception mode [14]; influence of OVS [15]) or by data reconstructions (aliasing artifacts or incomplete deapodization to suppress aliasing artifacts) [16,17]. In MRI applications that focus on the detection or delineation of objects or structures, such intensity distortions are of minor importance. However, for quantitative data evaluation performed in this study, an intensity recalibration was used assuming a uniform signal distribution at the beginning of the drying process.

2.4. Microscopic scale: microstructure observations by ESEM

The observations at the surface of alumina and kaolin samples were performed at the grain scale with an Environmental Scanning Electron Microscope (ESEM), model Quanta 450 FEG, supplied by FEI. The relative humidity was controlled close to the sample surface, and reduced from 100% step by step to observe the effect of drying. The relative humidity was controlled by setting the temperature of the sample holder to 2 °C, and the water vapour pressure in the chamber to 700 Pa which corresponds to 100% relative humidity. Reducing the pressure below 700 Pa then decreases the relative humidity. Likewise, a sample dried beforehand in an oven at 110 °C for 24 h was also observed in the same ESEM.

3. Results and discussion

3.1. Alumina P172SB samples

3.1.1. Weight loss and linear shrinkage

The weight loss and the simultaneous shrinkage of drying alumina P172SB samples as a function of time are shown respectively in Fig. 3 and Fig. 4.

At the beginning of drying, the material should be constituted uniquely of the solid and water. It can be noted that the water distribution is uniform throughout the sample as shown in the first profile of Fig. 4 (0 h). Also based on Fig. 3, we can differentiate two periods of drying. The first one lasts approximately 3 h which coincides with the major shrinkage and the second corresponds to the rest of the drying time. In the situation of slow drying, involving higher relative humidity and temperatures close to ambient, a continuous layer of water covers the surface of the sample throughout the CRP. Then the water evaporated from the surface and physical movement of the liquid/air interface leads to a redistribution of the water/particle system to maintain a uniform water concentration. In our study with one side exposed to drying, it is observed in Fig. 4 that even after 3 h of drying, the water content in the four sub-samples remains the same. However for drying duration of 4 h or more, a gradient in water concentration occurs and exhibits a maximum after 10 h. There is a difference of 25% in the water contents of sub-samples 1 and 2 while sub-samples 3 and 4 reveal

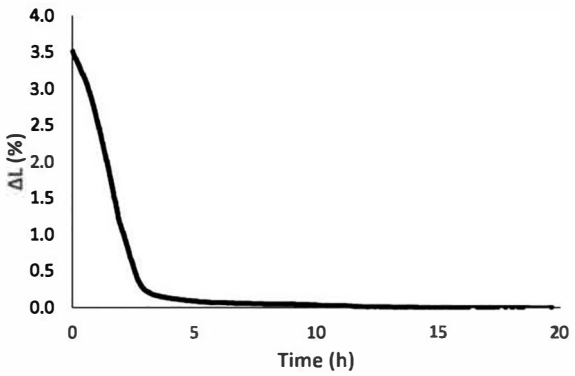

Fig. 3. Measured shrinkage of alumina P172SB sample as a function of time at 40 °C in ambient relative humidity.

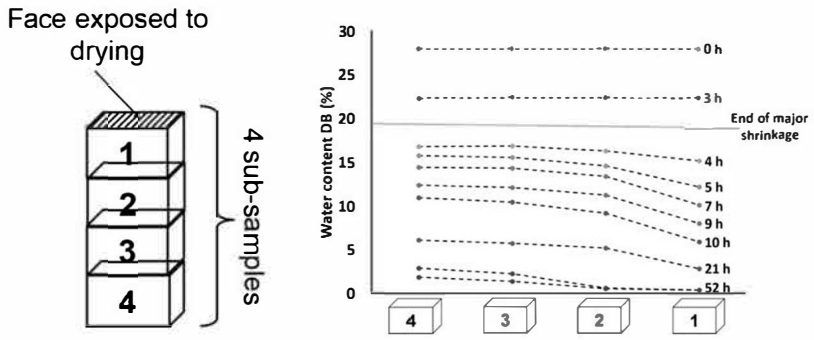

Fig. 4. Water content of alumina P172SB sub-samples after different drying times, at 40 °C in ambient relative humidity.

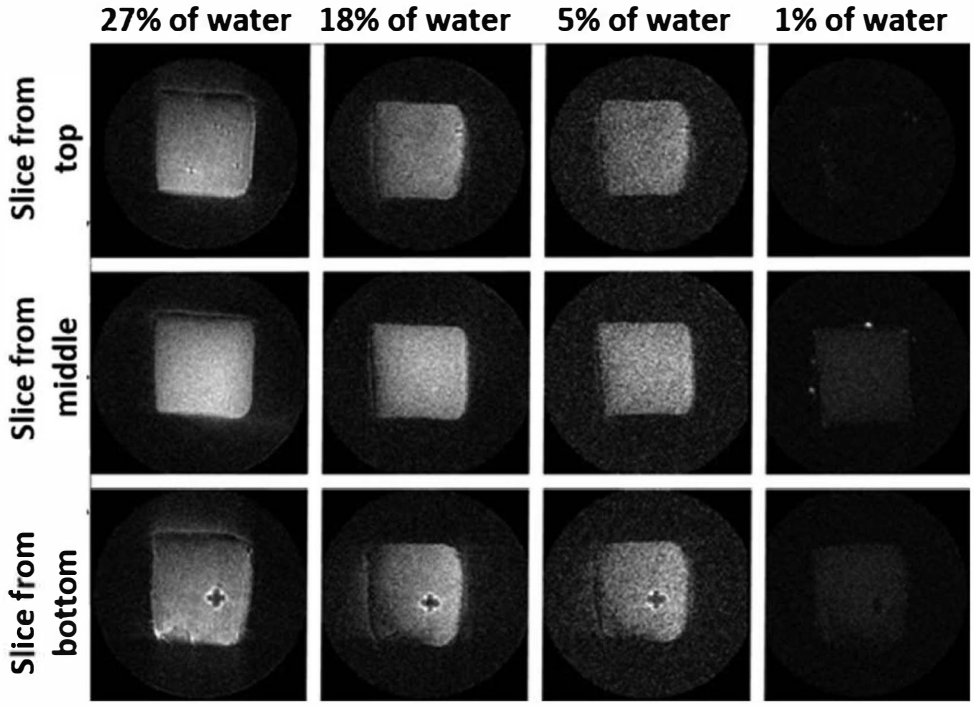

Fig. 5. Magnetic resonance images of an alumina P172SB sample, at different positions for total water contents of 27%, 18%, 5% and 1%.

only a small difference. As the outer part of the ceramic green body becomes completely dry, the steepest part of the gradient (drying front) moves towards the interior as shown by the curve obtained after 52 h.

3.1.2. ZTE magnetic resonance imaging

MRI images of the materials at various stages in drying are presented in Fig. 5. Three slices were chosen in order to illustrate how water is distributed within materials at different positions (from the top to the bottom). In this sample, only one face is exposed to the drying atmosphere while the others are covered with a plastic film. So in this situation the water migration should principally be in one direction. The first observation shows that the pixel intensity in the images for the top, middle and bottom positions, is greatest at the beginning of the drying process (1st column in Fig. 5). Then as drying progresses, the gray levels decrease, meaning that the amount of water decreases. Moreover, the images clearly reveal the phenomenon of shrinkage by the reduction of area of the squares during drying. For example, the square size at the beginning is about 4 cm^2 reducing to 3.69 cm^2 after drying is achieved. It corresponds to approximately 4% of linear shrinkage, which is very close to the value revealed in Fig. 3.

For further insight, results obtained by MRI were subsequently analyzed using an open-source software ParaView.5.4.1, to calculate averaged pixel concentration profiles, which should depict the water distribution. A vertical profile is chosen along the central axis of samples for the entire length, with averages made for cross sectional dimensions of 4 mm × 4 mm (Fig. 6). These profiles of average pixel intensities are shown in Fig. 7 at different times in the drying process. In this set of trials, the drying was accelerated by placing the sample on a hot plate at 50 °C and exposing the remaining 5 faces to the atmosphere.

The first observation is that the overall concentration in water decreases with time as expected. However, the first profile recorded after one hour of drying shows a reduced pixel intensity towards the top and bottom faces of the sample. Even if the drying conditions are different, this result is surprising since the distribution of water should be initially uniform as witnessed by the weight measurements of sub-samples

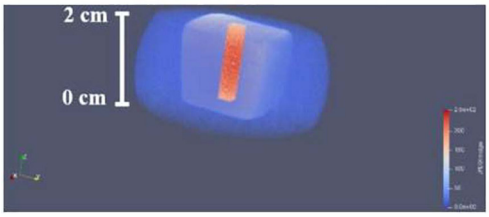

Fig. 6. Representation of the parallelepiped cut using Paraview software.

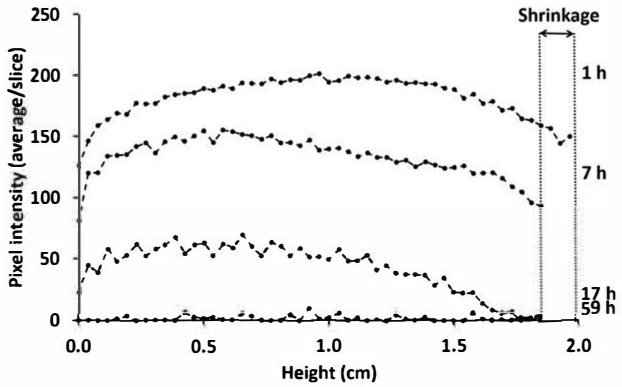

Fig. 7. Profile curves of the parallelepiped cut as a function of sample height for different drying times. Sample placed on a hot plate at 50 °C and with 5 faces exposed to air.

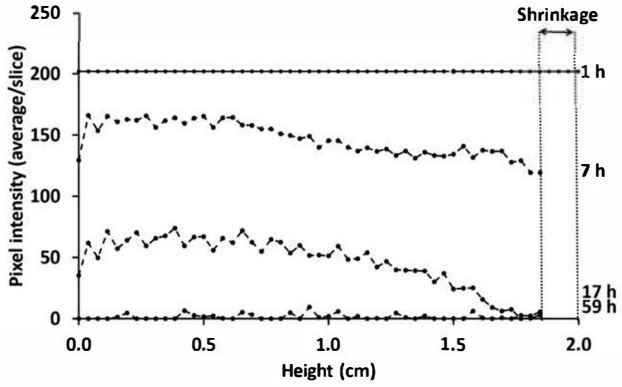

Fig. 8. Recalibrated profile curves of the parallelepiped cut as a function of sample height for different drying times. Note: the drying conditions are not the same as the weight measurements shown in Fig. 4.

(Fig. 4). Two possible explanations are considered. The forming process by casting could yield a crust towards the exterior of the sample but this does not seem consistent with the weight measurement of sub-samples discussed previously. Secondly, probing of water concentration by NMR measurements is less sensitive towards the outside of the sample chamber. It is indeed known that ZTE-MRI images of objects with constant spin density will often exhibit non-constant signal intensities across the object, with a trend of decreasing signal intensity with increasing distance from the image center. This problem arises from the specific way of data acquisition and reconstruction as described in Section 2.3. However, since the distribution of water in the sample is assumed to be uniform for the profile obtained after one hour of drying, the subsequent profiles can be recalibrated in relation to it, as shown in Fig. 8. The visualization of the behaviour then seems clear in the profile taken after 7 h of drying with the appearance of a gradient in water concentration for the top half of the sample (drying front) while the concentration remains uniform in the bottom half. It can be noted in the third profile that the local fluctuations of water content have increased, consistent with complete emptying of some but not all of the pores in a given volume element. Finally a uniform baseline signal of almost zero intensity is obtained for the dry sample (59 h of drying).

3.1.3. *ESEM observations*

The environmental scanning electron microscope was used to observe the surface of the samples at the micron scale of the grains and pores during drying. Though the experimental conditions inside the microscope chamber in terms of temperature and vapour pressures are some what different to the other two methods as explained in Section 2.4, the basic situation of progressively extracting water out of the ceramic green body is retained. Compared to the starting conditions of 2 °C and 700 Pa, this was achieved by progressively reducing the pressure to 500 Pa.

Observations of the drying process for alumina-P172SB surface are presented in Fig. 9 and Fig. 10. Micrographs of Fig. 9 show the evacuation of water in the same zone of the sample. The different

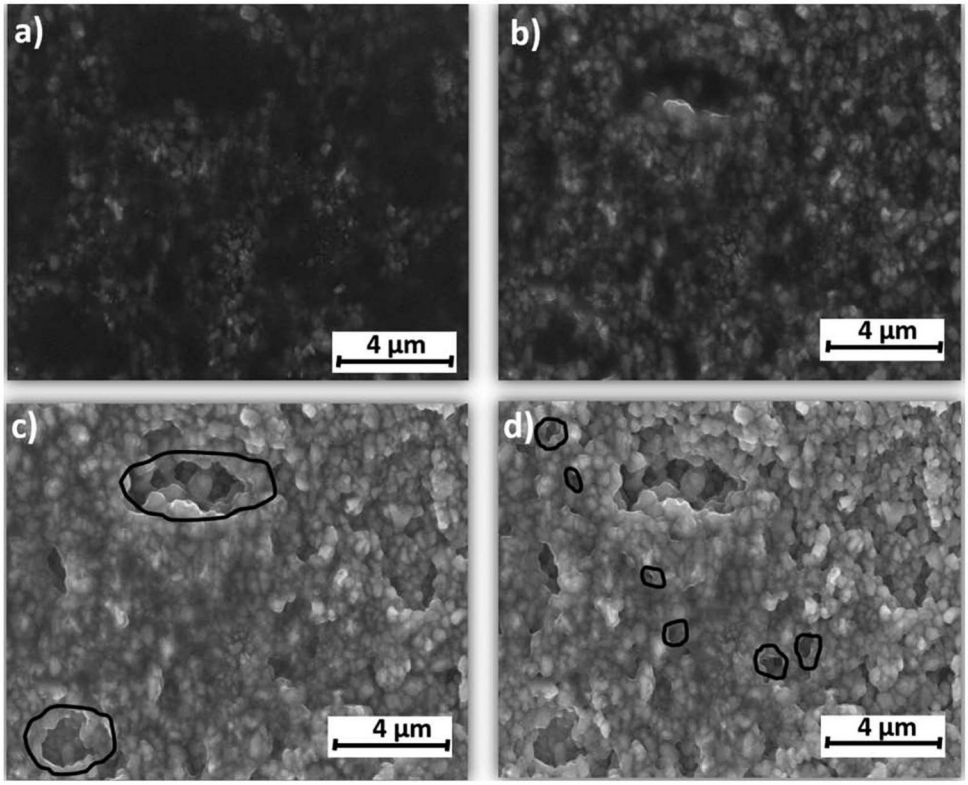

Fig. 9. ESEM micrographs of a chosen zone on the surface of an alumina-P172SB sample at various stages of drying. Micrographs (a) and (b) correspond to the CRP of drying with a continuous film of water surrounding grains. ((c) During the falling rate period with water evaporating from the large pores (marked by black lines). (d) Falling rate period, later in drying, with water emptying from the small pores (marked by black lines).

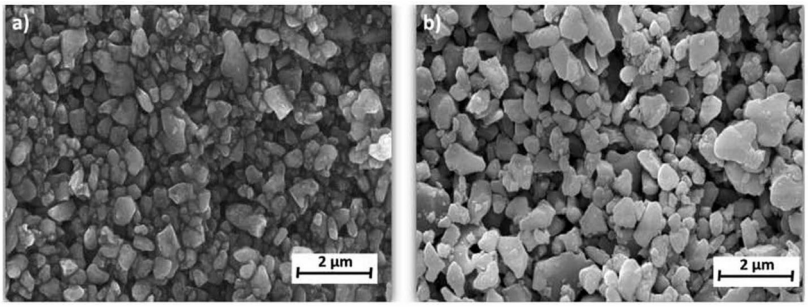

Fig. 10. ESEM micrographs of alumina-P172SB. (a) Sample at the end of drying in ESEM chamber. (b) Sample completely dried in an oven at 110 °C for 24 h.

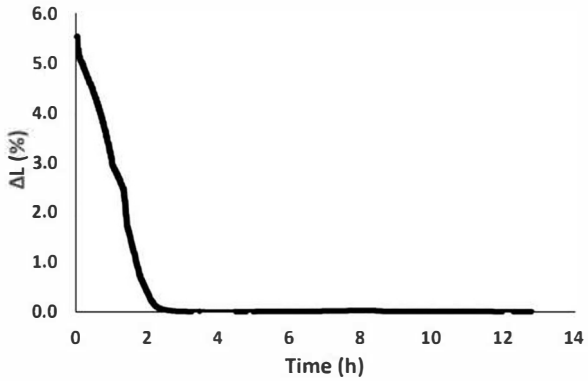

Fig. 11. Measured shrinkage of kaolin sample as a function of time at 40 °C and ambient relative humidity.

phenomena visible on the surface can be related to the different stages of drying. As one can see, in the first micrograph, water is the dark phase and it forms a continuous film around the grains. This is in agreement with the idea that in the early stages of drying, water evaporates from the surface (liquid–air interface) leading to shrinkage of the ceramic green body. Within the body, initially only solid-liquid interfaces exist.

The second micrograph corresponds to an advancement in the drying process, compared to the first micrograph, where the area occupied by the dark phase is reduced, meaning that the water level has decreased. It can also be noticed that grains are closer to each other which is directly related to shrinkage. In practice, the end of shrinkage is observed during the ESEM experiment when grains stop moving across the field of vision. This occurs between micrographs (b) and (c) of Fig. 9. After the shrinkage step, water starts first to evaporate from the larger pores and then the smaller pores are emptied later on during the drying process (Fig. 9(c) and (d). These observations are consistent with literature in the description of relations between the driving forces during drying and the tension in the liquid [6], which is strongly related to pore size. Capillary action ensures that the small pores near to the surface stay filled until all larger pores of the sample are drained. However, in Fig. 9(d) when all of these pores are essentially empty, some remaining moisture can be found located next to grain-grain interfaces. For the sample dried at 110 °C, presented in micrograph (b) of Fig. 10, it can be clearly seen that water located at interfaces between

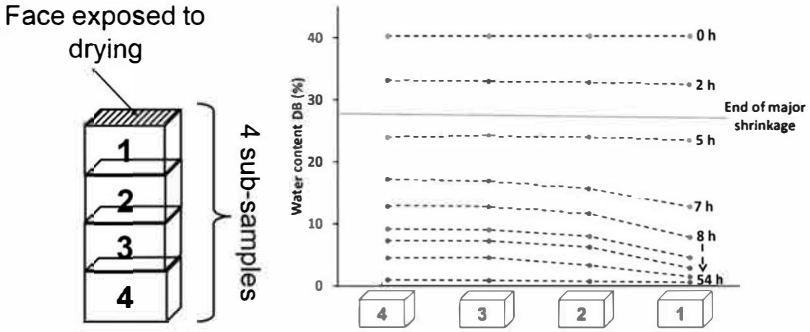

Fig. 12. Water content of kaolin sub-samples after different drying times, at 40 °C in ambient relative humidity.

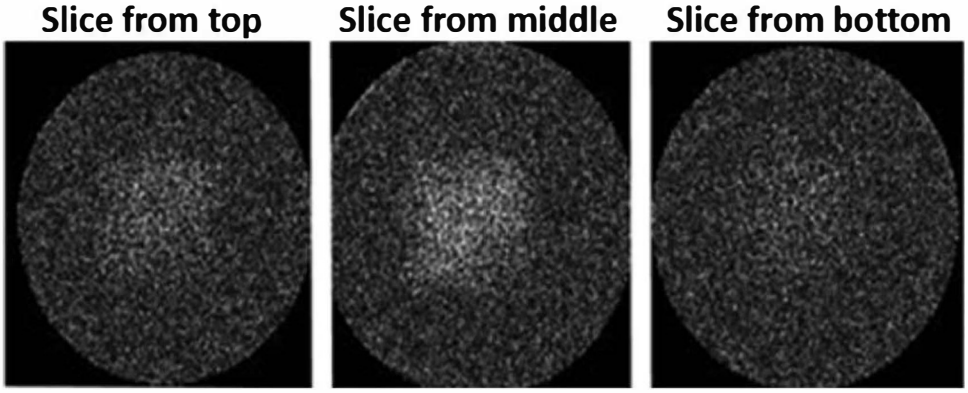

Fig. 13. MR images of kaolin for different positions at the end of drying.

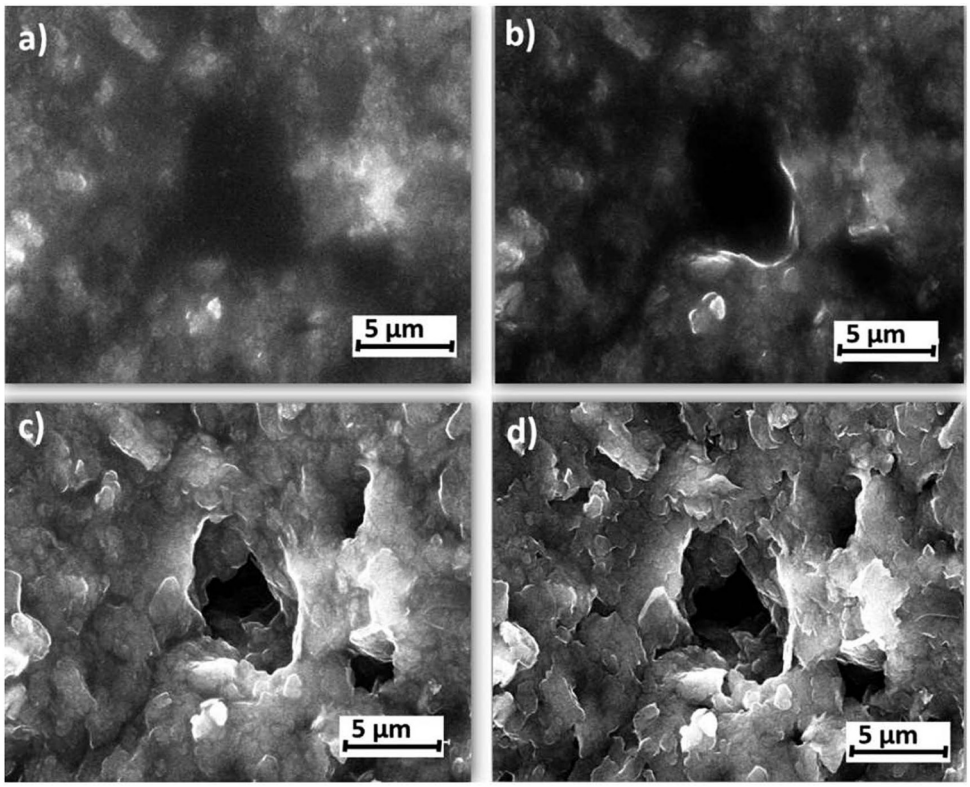

Fig. 14. ESEM micrographs of a chosen zone on the surface of a kaolin sample at various stages of drying. Micrographs (a) and (b) correspond to the CRP of drying with a continuous film of water surrounding grains. (c) Falling rate period with water evaporating from the large pores. (d) Further drying reveals emptying of water from the small pores.

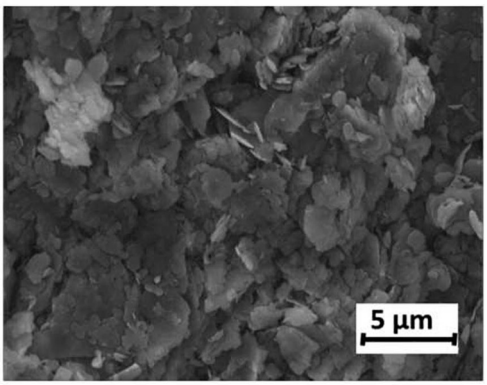

Fig. 15. ESEM micrograph of a kaolin sample completely dried in an oven at 110 °C for 24 h.

Table 2
Estimation of the diffusion coefficient values of water through an alumina P172SB sample at different times during drying (* indicates interpolated values).

Time (h)	$J_{x=0}$ (mol m^{-2} s^{-1})	$\frac{\Delta C}{\Delta x}$ (mol m^{-4})	D (m^2 s^{-1})
3	4.9×10^{-2}	2.1×10^{4}	2.3×10^{-6}
4	4.8×10^{-2}	1.3×10^{5}	3.8×10^{-7}
5	$^{*}3.6 \times 10^{-2}$	2.7×10^{5}	5.7×10^{-8}
7	$^{*}2.5 \times 10^{-2}$	3.6×10^{5}	3.5×10^{-8}
10	1.1×10^{-2}	3.6×10^{5}	3.1×10^{-8}
14	4.9×10^{-3}	3.1×10^{5}	1.6×10^{-8}
21	3.7×10^{-3}	2.6×10^{5}	1.4×10^{-8}

grains has been completely removed. It has been deduced in a previous paper that this small quantity of water located at the contact between grains can have strong influence on material properties. The study showed that the thermal conductivity decreased strongly during the last phase of drying [18].

3.2. Kaolin samples

Despite the difference of morphology between kaolin and alumina, i.e. spherical form of grains for alumina and platelets for kaolin, many aspects of the general behaviour during drying of kaolin samples are similar to alumina. Linear shrinkage as a function of time and the profiles of water concentration obtained by weight measurements of sub-blocks are respectively presented in Fig. 11 and Fig. 12. During the initial shrinkage, which takes place in the first 2 h of drying, no gradient in water content within samples is detected as shown in Fig. 11. Later on in the drying process, a gradient in water concentration develops, reaching a maximum value after 8 h. The MRI observations also reveal the progression of a drying front once the shrinkage stage is completed.

A notable difference for the kaolin samples with the MRI technique is that even at the end of drying quite a strong signal remains as shown in Fig. 13. This ^{1}H signal is expected because of the presence of OH groups in kaolinite which give rise to a residual signal [19].

Observations of a kaolin sample during drying using the ESEM are presented in Fig. 14 and Fig. 15. As for alumina samples, during the first stage of drying (first and second micrographs), the grains are surrounded by water. Only liquid/solid and liquid/gas interfaces exist. Then during the falling rate period, water starts to evaporate from the larger pores before the smaller ones, similar to the observations for alumina.

3.3. Estimation of diffusivity for water transport in drying ceramic green body

In this final section, order of magnitude estimates of the diffusivity values for water transport in the drying body are made. As a useful simplification, the situation of one dimensional transport after the shrinkage stage is considered. From a mass balance made at the sample face exposed to air at $x = 0$, the outgoing water flux $J_{x=0}$ [mol m^{-2} s^{-1}] can be written as [20,21]:

$$J_{x=0} = -D\frac{\partial C}{\partial x} \quad (3)$$

where D is the diffusion coefficient in $m^2 s^{-1}$, C is the water concentration in mol m^{-3} in the volume element next to the interface and x is the position coordinate in m. This is similar to an expression for Fick's law within the body. An approximate value for the upper limit of the diffusion coefficient D can then be given by the relation.

$$D = \frac{J_{x=0}}{\frac{\Delta C}{\Delta x}} \quad (4)$$

where $\frac{\Delta C}{\Delta x}$ refers to the difference in water concentration of the first two sub-samples per unit length next to the drying face in Fig. 2 and the sign has been dropped. In reality the local concentration gradient may be steeper next to the interface. The diffusion flux corresponds to the amount of evaporated water per unit area of exposed drying surface during a given time period described by the relation:

$$J_{x=0} = \frac{1}{S}\frac{\Delta C}{\Delta t} \quad (5)$$

where ΔC refers to the change in average concentration of the complete sample over time Δt and S is the area of the exposed face.

In the case of the alumina-P172SB samples, shrinkage is essentially finished after 3 h of drying. Using Eqs. (4) and (5), diffusion coefficient values were calculated from 3 h to 21 h of drying, since a concentration gradient in the first two subsamples is revealed during this stage (Table 2). The evaporation rate from the drying surface was evaluated over a time difference of 2 h by interpolation of the average mass values for the complete sample.

First, it can be noted that the values of the diffusion coefficient of water lie between a value of $2.3 \times 10^{-6}\ m^2 s^{-1}$ just after the end of the CRP and a value of $1.4 \times 10^{-8}\ m^2 s^{-1}$ after 21 h of drying when 5% of water still remains within the sample. These estimations are in rough agreement with values found in literature. As an example, for water evaporation from a porous alumina pellet the diffusion coefficient of water within the pellet was deduced to be $5 \times 10^{-8}\ m^2 s^{-1}$ from the concentration profile evaluated by MRI measurements [11]. In addition, other studies, based on weight measurements to estimate the diffusion coefficients for brick materials, have showed similar dependence on moisture content during drying and values which are of the same order of magnitude [22,23]. Second, the initial large value of the diffusion coefficient should come as no surprise given that, at high water amounts within the material, capillary forces are the main mechanism transporting water. The progressive decrease in diffusion coefficient value, with drying time and water amount, is then consistent with a change in the dominant transport mechanism towards diffusion of water vapour through the pores to the outside surface.

A simple attempt was made to test this explanation by altering the microstructure of the drying ceramic and hence modify the two transport mechanisms. Two alumina powders were compared: P172SB with small grains (0.4 μm) and P152SB with larger grains (1.3 μm). Presumably the presence of smaller pores and particles is promoted in P172SB compared to P152SB. First of all the total mass losses of the alumina samples were followed in the same conditions of drying, i.e. at the same humidity and at similar temperatures. The drying rates were then calculated from water loss over time per unit of area exposed to drying and are plotted as a function of moisture content in Fig. 16.

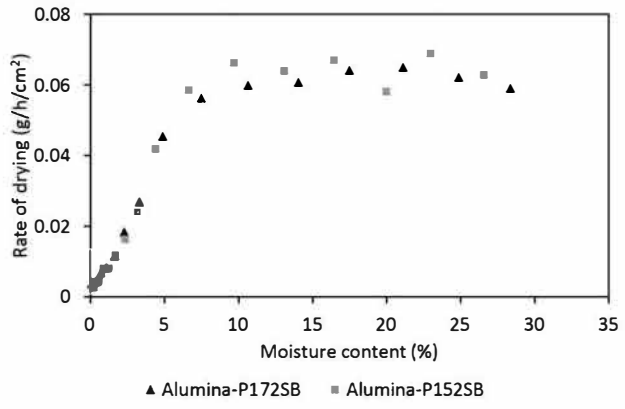

Fig. 16. Rate of drying as a function of the moisture content for two alumina powders at 40 °C and 30% of relative humidity.

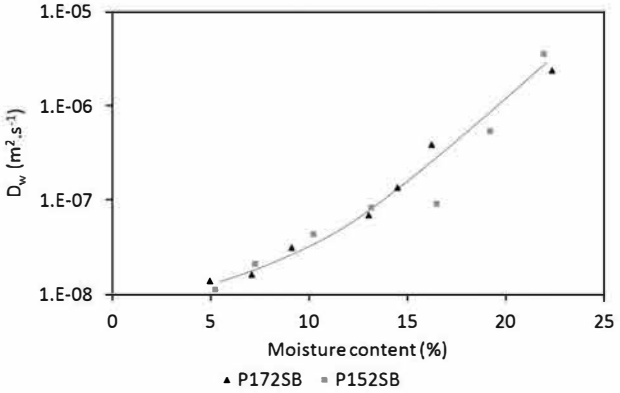

Fig. 17. Estimated diffusion coefficient as a function of the moisture content for two alumina powders P172SB and P152SB.

Despite the increase in particle size between the alumina powders (P152SB three times larger than P172SB), no significant difference in drying behaviour is revealed, especially after the constant rate period is completed (moisture content less than 8%).

Furthermore, the estimation of diffusion coefficients for P152SB, via the weighing of sub-samples yields again a strong dependence on moisture content as shown in Fig. 17. The two data sets can not be distinguished within uncertainty, suggesting reproducibility and that the two pore size distributions are not sufficiently different. More refined evaluation might yield differences at the lowest moisture contents, corresponding to the emptying of the smallest pores.

Even if no particular effect due to grain size difference in the alumina powders was detected, these simple estimations of diffusion coefficient represent an interesting start in the comprehension of the role of this parameter in drying of ceramic bodies. It should be possible to obtain more refined values of the diffusion coefficient by constructing a numerical model for the drying of a green ceramic body, which predicts internal concentration profiles to compare to experimental data.

4. Conclusion

Although the mechanisms of drying have been investigated in the past, rather few studies using modern techniques have been devoted to the spatial distribution and the localization of water at the grain scale. This work brings new information but basically confirms the general picture of drying established in the literature. For "slow" drying corresponding to removal of water by natural convection, during the first stage involving shrinkage, the distribution of water in the ceramic body is uniform. Then during the second stage of drying, when the body volume is fixed and water evaporates from the pores in the interior of the body, the distribution of water within the sample varies with position. A gradient in water concentration is revealed between emptied zones next to the drying face(s) and the body interior where water is removed more slowly. In the final stage of drying, the residual water is localized in the zones next to the solid-solid contacts between particles. These experimental results not only provide insight into the mechanisms, but also give information on the evolution of the effective diffusion coefficient of water in the drying ceramic body. Furthermore, such data associated with that concerning the thermal conductivity obtained

in previous work, will allow us to construct a robust numerical model to describe the behaviour of a green ceramic body during drying.

Acknowledgments

Siham Oummadi thanks the Limousin Region for financial support of her PhD as well as the JECS Trust for a mobility bursary for the studies on the MRI measurement at the University of Bremen.

References

[1] M. Kornmann, Clay Bricks and Roof Tiles, Manufacturing and Properties, Société de l'industrie minérale, Paris, 2007 OCLC: 733836312.
[2] J. Kiennemann, T. Chartier, C. Pagnoux, J.F. Baumard, M. Huger, J.M. Lamérant, Drying mechanisms and stress development in aqueous alumina tape casting, J. Eur. Ceram. Soc. 25 (9 (June)) (2005) 1551–1564.
[3] Loi de transition énergétique pour la croissance verte. Journal Officiel du 18 août 2015.
[4] D. Fuks, G.E. Shter, M. Mann-Lahav, G.S. Grader, Crack-free drying of ceramic foams by the use of viscous cosolvents, J. Am. Ceram. Soc. 93 (11 (November)) (2010) 3632–3636.
[5] R.W. Ford, Ceramics Drying, Elsevier, 2013 October.
[6] G.W. Scherer, Theory of drying, J. Am. Ceram. Soc. 73 (1 (January)) (1990) 3–14.
[7] T.K. Sherwood, The drying of solids—I, Ind. Eng. Chem. 21 (1 (January)) (1929) 12–16.
[8] T.K. Sherwood, The drying of solids—II, Ind. Eng. Chem. 21 (10 (October)) (1929) 976–980.
[9] T.K. Sherwood, The drying of solids—III. Mechanism of the drying of pulp and paper, Ind. Eng. Chem 22 (2) (1930) 132–136.
[10] E. Keita, P. Faure, S. Rodts, P. Coussot, MRI evidence for a receding-front effect in drying porous media, Phys. Rev. E 87 (6 (June)) (2013) 062303.
[11] I.V. Koptyug, S.I. Kabanikhin, K.T. Iskakov, V.B. Fenelonov, L. Yu Khitrina, R.Z. Sagdeev, V.N. Parmon, A quantitative NMR imaging study of mass transport in porous solids during drying, Chem. Eng. Sci. 55 (9 (May)) (2000) 1559–1571.
[12] S. Hafner, Fast imaging in liquids and solids with the Back-projection Low Angle ShoT (BLAST) technique, Magn. Reson. Imag. 12 (7) (1994) 1047–1051.
[13] M. Weiger, K.P. Pruessmann, F. Hennel, MRI with zero echo time: hard versus sweep pulse excitation, Magn. Reson. Med. 66 (2 (August)) (2011) 379–389.
[14] M. Weiger, K.P. Pruessmann, MRI with Zero Echo Time, eMagRes, American Cancer Society, 2012.
[15] W. Dreher, I. Bardenhagen, L. Huang, M. Bäumer, On the suppression of background signals originating from NMR hardware components. Application to zero echo time imaging and relaxation time analysis, Magn. Reson. Imag. 34 (3 (April)) (2016) 264–270.
[16] M.A. Bernstein, K.F. King, X.J. Zhou, Handbook of MRI Pulse Sequences, Elsevier Academic Press, 2004 Chapter 13.2 (gridding reconstruction).
[17] J.M. Pauly, Gridding & the NUFFT for non-cartesian image reconstruction, Proceedings of the 21st Annual Meeting of ISMRM, Salt Lake City, Utah, 2013, p. 45.
[18] B. Nait-Ali, S. Oummadi, E. Portuguez, A. Alzina, D.S. Smith, Thermal conductivity of ceramic green bodies during drying, J. Eur. Ceram. Soc. 37 (4 (April)) (2017) 1839–1846.
[19] S. Hayashi, T. Ueda, K. Hayamizu, E. Akiba, NMR study of kaolinite. 1. Silicon-29, aluminum-27, and proton spectra, J. Phys. Chem. 96 (26 (December)) (1992) 10922–10928.
[20] J.M. Philibert, Atom Movements – Diffusion and Mass Transport in Solids, EDP Sciences, 2012 December.
[21] F.P. Incropera, D.P. Dewitt, T.L. Bergma, A.S. Lavine, Fundamentals of Heat and Mass Transfer, John Wiley & Sons, 2007.
[22] U. Telljohann, K. Junge, E. Specht, Moisture diffusion coefficients for modeling the first and second drying sections of green bricks, Drying Technol. 26 (7 (July)) (2008) 855–863.
[23] A.J.J. van der Zanden, M.H. de Wit, A procedure to measure the diffusion coefficient of water in brick as a function of the water concentration, Drying Technol. 30 (5) (2012) 526–534.